Thermal conduction from microcantilever heaters in partial vacuum

Jungchul Lee, Tanya L. Wright, Mark R. Abel, Erik O. Sunden, Alexei Marchenkov et al.

Citation: J. Appl. Phys. **101**, 014906 (2007); doi: 10.1063/1.2403862
View online: http://dx.doi.org/10.1063/1.2403862
View Table of Contents: http://jap.aip.org/resource/1/JAPIAU/v101/i1
Published by the American Institute of Physics.

Thermal conduction from microcantilever heaters in partial vacuum

Jungchul Lee, Tanya L. Wright, Mark R. Abel, and Erik O. Sunden
George W. Woodruff School of Mechanical Engineering, Georgia Institute of Technology, Atlanta, Georgia 30332

Alexei Marchenkov
School of Physics, Georgia Institute of Technology, Atlanta, Georgia 30332

Samuel Graham and William P. King[a)]
George W. Woodruff School of Mechanical Engineering, Georgia Institute of Technology, Atlanta, Georgia 30332

(Received 26 September 2006; accepted 20 October 2006; published online 9 January 2007)

This paper reports the thermal and electrical characteristics of a heated microcantilever in air and helium over a wide range of pressures. The cantilever heater size modulates thermal conductance between the cantilever and its gaseous surroundings; and the Knudsen number, Kn characterizes this thermal conductance. When $\mathrm{Kn}<1$, thermal transport from the cantilever heater depends on gas pressure, and when $\mathrm{Kn}>1$, thermal transport from the cantilever heater remains constant. This measurement of thermal conductance around $\mathrm{Kn}=1$ could aid the design and analysis of Pirani sensors and other microscale thermal sensors and actuators. © *2007 American Institute of Physics*. [DOI: 10.1063/1.2403862]

I. INTRODUCTION

Thermal transport in regimes of size comparable to the energy carrier mean free path can differ significantly from thermal transport in bulk regimes[1] and the relevant physics govern both microcantilever heaters in partial vacuum and the operation of micron-sized Pirani gauges.[2] Pirani pressure sensors consist of a resistive heating element, having a temperature-dependent electrical resistance, mounted a finite distance from a heat sink. The typical Pirani sensor exploits the pressure-dependent molecular collision rate in the gap between the heater and heat sink, such that enhanced cooling can be observed with increasing pressure. The dynamic range of the sensor is limited by the saturation of thermal conductance of the gas medium, which depends on the molecular collision rate. While micro-Pirani gauges are well understood, somewhat less well studied are microelectromechanical system (MEMS) devices with an integrated heater where the heater element is small compared to the mean free path of the gas environment. The Knudsen number, $\mathrm{Kn}=\lambda/l$, is the ratio of the energy carrier mean free path λ to the size of either the heater or the constriction, l. Kn is a measure of molecular collision rate and can characterize the operation of Pirani gauges and other MEMS devices having integrated heaters.[3]

Atomic force microscope (AFM) cantilevers having integrated resistive heaters were originally developed for data storage,[4,5] but have since been shown to be useful for sensing,[6,7] nanoscale manufacturing,[8] and microscale thermophysical measurements.[9] Previous published studies of thermal interactions between a heated cantilever and its surroundings have shown that gas-gas and gas-solid molecular collisions in the gap between a heated microcantilever and a surface can play a significant role in the thermal conductance between the two bodies and can exert Knudsen forces on the cantilever, inducing cantilever bending.[7,9] For decreasing pressure, the gaseous molecular mean free path becomes long and these effects may become particularly acute. However, there are no published reports on thermal transport between an AFM cantilever having an integrated heater and a vacuum environment.

This paper reports experimental observations of heat flow from microcantilever heaters into air or helium for $10^{-2}<\mathrm{Kn}<10^{4}$ where Kn is based on the cantilever heater size. When $\mathrm{Kn}>1$, thermal conduction from the cantilever heater to its environment is constant. However, when $\mathrm{Kn}<1$, thermal conduction from the cantilever heater into the gaseous environment depends gas pressure. The heat transfer efficiency is thus characterized by the molecular collision rate between the cantilever heater and the surrounding gas. Unlike previous reports on heat transport between a heated cantilever and a vacuum environment, the present study measures both temperature and heating power inside the cantilever, allowing direct measurement of thermal conductance.

II. EXPERIMENT

The experiments were performed using heatable AFM cantilevers fabricated in our group following a fabrication process modified from previous reports.[10] Figure 1 shows scanning electron microscope (SEM) and infrared (IR) microscope images of a heatable AFM cantilever. The SEM image was made with the cantilever unheated and at low vacuum, and the IR image was made with the cantilever heated, in air at ambient pressure. The cantilever was made from single-crystal silicon that had two regions of phosphorus doping. The cantilever legs were phosphorus doped to a concentration near 1×10^{20} cm^{-3}, and thus had low resistivity close to 8×10^{-4} Ω cm. The cantilever heater region was phosphorus doped to a concentration near 1

a)Electronic mail: william@me.gatech.edu

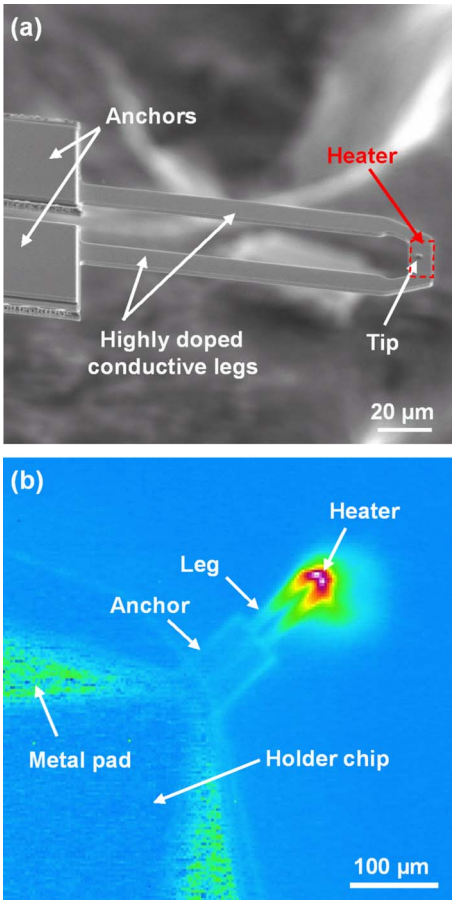

FIG. 1. (Color online) (a) Scanning electron microscope image of a silicon microcantilever having an integrated heater. The fabricated cantilever is "U shaped" such that it forms a continuous electrical path. The region near the cantilever free end is a highly resistive heater and the legs have lower electrical resistance such that they can act as electrical leads. (b) IR micrograph of a heated AFM cantilever in air at STP. The image is approximately 0.5 mm^2.

$\times 10^{17}$ cm^{-3}, and thus had resistivity close to 9×10^{-2} Ω cm. The heatable cantilever was 100 μm long with two 10 μm wide legs and the heater was approximately 8 $\times$16 μm in size. Overall the cantilevers had electrical resistance near 1.8 kΩ, with about 90% of the cantilever electrical resistance due to the high resistivity heater region. When electrical current passes through the cantilever, the high resistance region at the end of the cantilever is resistively heated. When the cantilever is operated in a quiescent environment, solid conduction through the cantilever legs and gas conduction through the adjacent gas surroundings balance the heat generated near the cantilever free end.

The experiment began with electrical characterization of the heated cantilever. For all of the experiments, the cantilever was operated in series with a precision power resistor with a value of 10 kΩ. The simple bridge circuit consisting of the cantilever and the series resistor was driven with dc voltage excitation, and the voltage across the series resistor was monitored.[11] Figure 2 shows the cantilever electrical resistance as a function of heating power in laboratory air at ambient pressure. The cantilever resistance first increases with increasing power as electron scattering increases with increasing temperature. At heating power of about 3.7 mW,

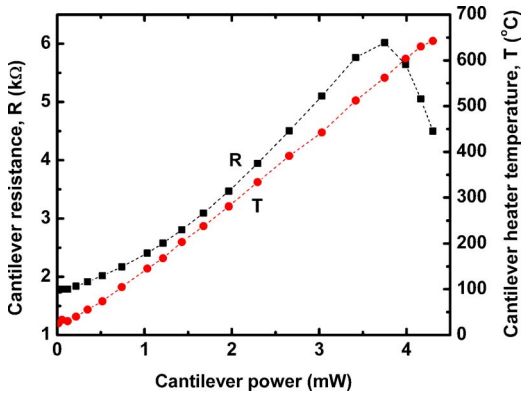

FIG. 2. (Color online) Cantilever electrical resistance and cantilever heater temperature as a function of heating power in air at 1 atm.

the cantilever resistance decreases with increasing power, as the thermally generated intrinsic carriers outnumber the background carriers. This thermal runaway behavior is characteristic of doped silicon and is typically observed during the characterization of these heated microcantilevers.[11,12] The temperature at which thermal runaway occurs is highly repeatable for a given cantilever and can be used as a convenient temperature calibration point. For this cantilever, the peak electrical resistance corresponded to 560 °C.

The cantilevers were temperature calibrated using Raman spectroscopy, which can measure the cantilever heater temperature to within 5 °C and with spatial resolution of 1 μm.[11,13] We have previously reported Raman spectroscopy for temperature calibration of silicon microstructures[13] and microcantilever heaters[11] and very briefly review the technique here. The measured Stokes peak shift is a linear function of temperature for doped silicon over the temperature range of interest.[13] When the cantilever is heated, lattice spacing and polarizability of silicon change and these affect Raman signature. Stokes peak corresponds to inelastic scattering when incident photons lose their energy due to photon-phonon interaction and this peak will be shifted to longer wavelength as device temperature increases. For a cantilever heater temperature in the range of 200–500 °C, the cantilever temperature coefficient of electrical resistance (TCR) is about 5.6×10^{-3}/°C. The cantilever TCR is about double that of platinum, and so the cantilever can be used as a very sensitive thermometer. Because about 90% of the cantilever resistance is the resistance of the cantilever heater region, the cantilever total electrical resistance is very close to the resistance of the cantilever heater. The cantilever total electrical resistance is thus a good indicator of the temperature in the cantilever heater region. Explained below in more detail, it is reasonable to assume that the temperature calibration of cantilever electrical resistance that was performed at ambient pressure can be broadly applied over a large range of pressures.[5,9,10] Figure 2 shows the cantilever temperature as a function of heating power. This calibration shows cantilever temperature between 25 and 650 °C, although it is possible to heat the cantilever above 1000 °C for several minutes without damage.[14] Over the temperature range measured, the cantilever temperature was linear with heating power, indicating that for operation in air at 1 atm, thermal

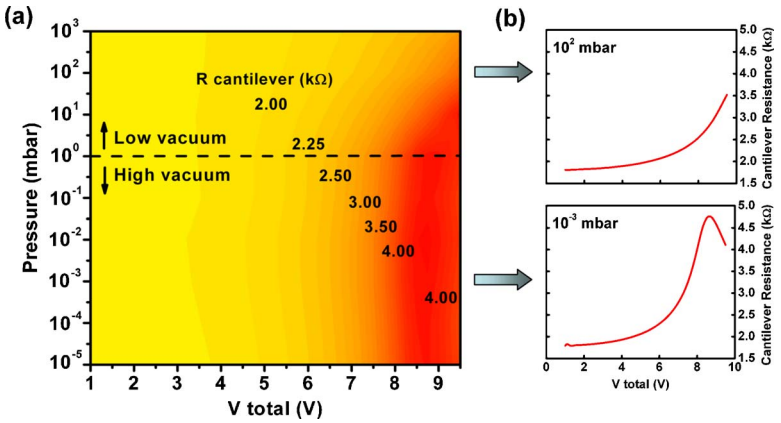

FIG. 3. (Color online) (a) Contour plot of electrical resistance of a heated AFM cantilever as a function of bias voltage and pressure in air. (b) Two representative plots of measured cantilever electrical resistance as a function of bias voltage at low vacuum (10^2 mbar) and high vacuum regimes (10^{-3} mbar).

radiation is not a significant mode of heat transfer. A detailed analysis of the heat transfer modes will be discussed later.

Six cantilevers were calibrated and prepared in a single package, to check the consistency of the experimental results. The package was placed in an ultrahigh vacuum (UHV) chamber capable of controlled pressure between 10^{-6} and 10^3 mbar. Since the cantilevers were positioned about 500 μm apart from the center of the bottom of the UHV chamber and about 25 cm away from the other surfaces, only the bottom surface of the UHV chamber and the nearby gas could act as conduction heat sinks. The chamber could be backfilled with different gases such that it was possible to modulate thermal properties of the gaseous environment near the cantilever. In this experiment, the gases were air and helium.

The UHV chamber was pumped down to 10^{-6} mbar at the start of the experiments. The chamber was slowly filled with gas, stopping at predetermined pressures. At this point, the cantilever was powered with a steady excitation voltage, and the cantilever resistance and power were recorded. Three measurements were made for every decade of pressure. The cantilever response was measured for chamber pressures between 10^{-5} and 10^3 mbar for air, and between 10^{-3} and 10^3 mbar for helium.

Figure 3 shows measured cantilever electrical resistance as a function of excitation voltage in air with pressure between 10^{-5} and 10^3 mbar. The contour plot of Fig. 3(a) shows two distinct pressure regimes of thermal coupling between the cantilever and environment. At low vacuum, the peak resistance occurred at a decreasing excitation voltage with decreasing pressure. However, the heated cantilever became insensitive to further pressure reduction at high vacuum. Figure 3(b) shows two representative cantilever electrical responses at 10^2 and 10^{-3} mbar, corresponding to low vacuum and high vacuum cantilever responses.

To compare power dissipation at a given pressure, Fig. 4(a) shows dissipated power in the cantilever as a function of gas pressure for both air and helium when the cantilever heater temperature was held at 400 °C. As expected, the cantilever could dissipate more power to the helium since helium thermal conductivity is higher than that of air at a given pressure. However, both air and helium show a crossover between 1 and 10 mbar where the dissipated power becomes pressure independent.

It is helpful to examine the pressure dependence of heat flow into the two gases used by considering the molecular mean free path. With the ideal gas assumption, the molecular mean free path can be calculated by $\lambda=(k_BT)/\sqrt{2}\pi Pd^2$ where k_B is the Boltzmann constant, T is temperature, P is pressure, and d is the effective diameter of the gas molecule.[3] The molecular collisions between the cantilever heater and the gaseous medium are expected to drop near Kn=1, and we presume that heater size modulates the thermal conduction between the cantilever heater and the environment.

Figure 4(b) shows dissipated power in the cantilever as a

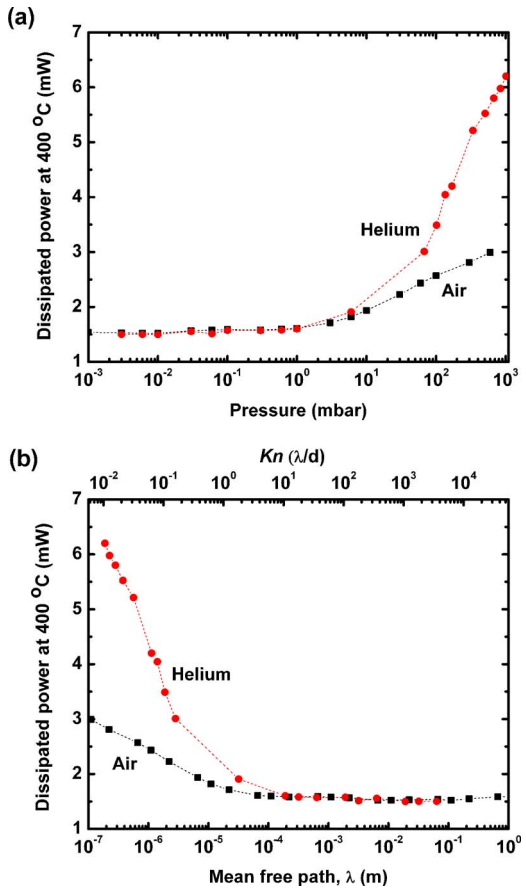

FIG. 4. (Color online) Dissipated power in a heated AFM cantilever as a function of (a) pressure and (b) gas mean free path and corresponding Kn number for both air and helium where the cantilever heater temperature is held at 400 °C.

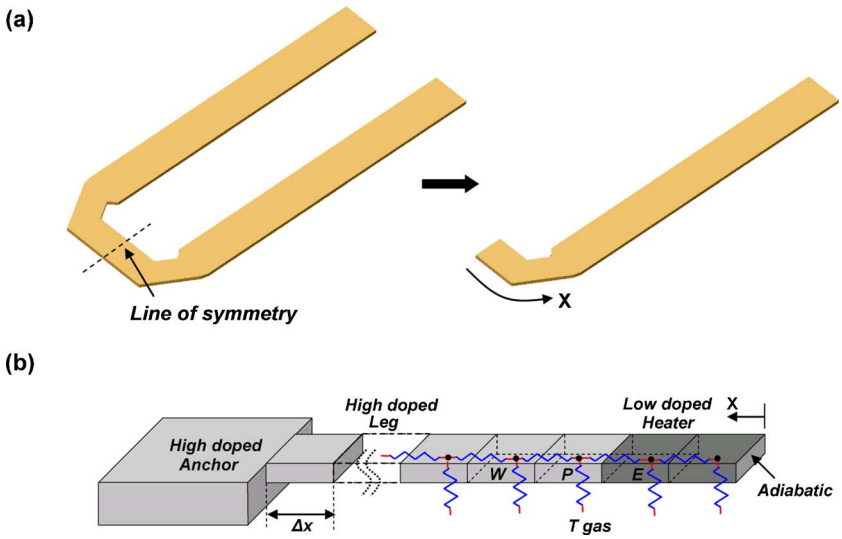

FIG. 5. (Color online) (a) "U-shape" cantilever structure showing line of symmetry. (b) One dimensional finite difference heat transfer model including solid conduction resistance between adjacent nodes and air conduction resistance.

function of calculated mean free path or corresponding Kn when the cantilever heater temperature was held at 400 °C. Figure 4(b) shows results for both air and helium. There is a transition from pressure dependence to pressure independence of thermal conduction from the cantilever heater at approximately 2×10^{-5} m which is close to the cantilever heater size. Although the thermophysical properties of helium are significantly different than the properties of air, the transition of the thermal response is near Kn=1 for both air and helium.

The observed transition from pressure dependence to pressure independence of the near Kn=1 can be explained as follows. When Kn is equal to or greater than 1, i.e., the size of the heater becomes comparable to the molecular mean free path, the character of the heat exchange between the heater and the gaseous medium changes from diffusive to stochastic, which is dominated by the frequency of the molecular collisions with the heater. While air and helium conductances may still show pressure dependence near Kn=1, their relative contribution to the overall conductance becomes negligible and undetectable.

To summarize the experimental observations: at high vacuum, thermal conduction to the gas was negligible compared to thermal conduction through the cantilever legs; at low vacuum, gas conductance increased such that higher power could be dissipated at a given temperature.

III. HEAT TRANSFER MODELING

A simple model for heat flow within and from the cantilever was developed to guide a deeper understanding of the thermal interactions between the cantilever and its gaseous environment. The heat transfer model employed the thermal resistance network shown in Fig. 5, following previously published analyses of heat transfer in heated microcantilevers.[5,15] Because the thermal resistance to heat flow away from the cantilever is greater than the thermal resistance to heat flow within the cantilever, it can be assumed that the cantilever temperature varies only along its length and does not vary across the cantilever width or thickness. A one-dimensional finite difference heat transfer simulation was employed, where the cantilever was divided into 216 nodes. Thermal conduction between adjacent nodes was calculated using Fourier's law.[16] Temperature-dependent thermal conductivity of doped silicon was adopted from literature values.[17] Each node was assigned a cantilever-gas thermal conductance, which was used as a fitting parameter. While the cantilever-gas conductance was constant for every position along the cantilever and independent of temperature, the heat flow from any given node into the surrounding gaseous medium was the product of the node temperature and the conductance. As was observed above, at 1 atm, heat transfer from the cantilever was linear with temperature over the entire temperature range, indicating that thermal radiation was small compared to thermal conduction. Natural convection was neglected as well; for micron-scale heat sources, buoyancy forces are not sufficiently large to overcome viscous forces. For each simulation, an energy balance was performed on the system to check that the heat generated was equal to the heat leaving the cantilever. The predictions closely matched analytical solutions for a test case that assumed a known cantilever-gas conductance.

Figure 6 shows the predictions for the temperature along the cantilever, along with measured temperature in the cantilever heater at 1 atm. When the cantilever was heated to 2.97 mW in air at 1 atm, the cantilever heater temperature was 400 °C and the cantilever electrical resistance was 4.61 kΩ. Because more than 90% of the cantilever electrical resistance occurs in the cantilever heater region, when the measured cantilever electrical resistance was 4.61 kΩ, the cantilever heater region was at 400 °C regardless of the fraction of heat that flowed into the nearby gas versus down the legs of the cantilever. In Figs. 6(a) and 6(b), local temperature along the cantilever changes exponentially[11] except near the heater region. The temperature drop along the cantilever is more significant with helium than with air due to the difference in thermal conductivity between the gases. As pressure decreases, the cantilever-gas conductance decreases, and less power is required to produce a fixed temperature.

Figure 7 shows measured and predicted conductances from the cantilever at 400 °C in air and helium, with good agreement between simulation and measurement. The ex-

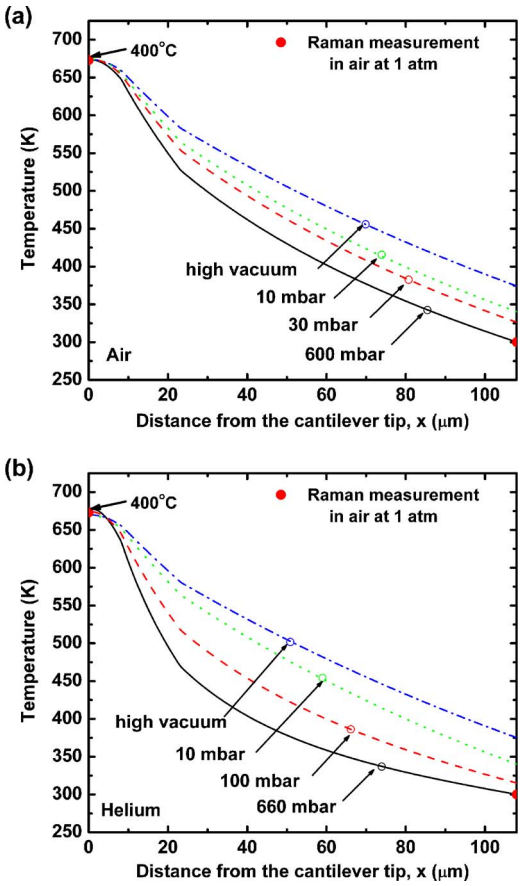

FIG. 6. (Color online) Simulated temperature distribution in the heated cantilever at different pressures in (a) air and (b) helium.

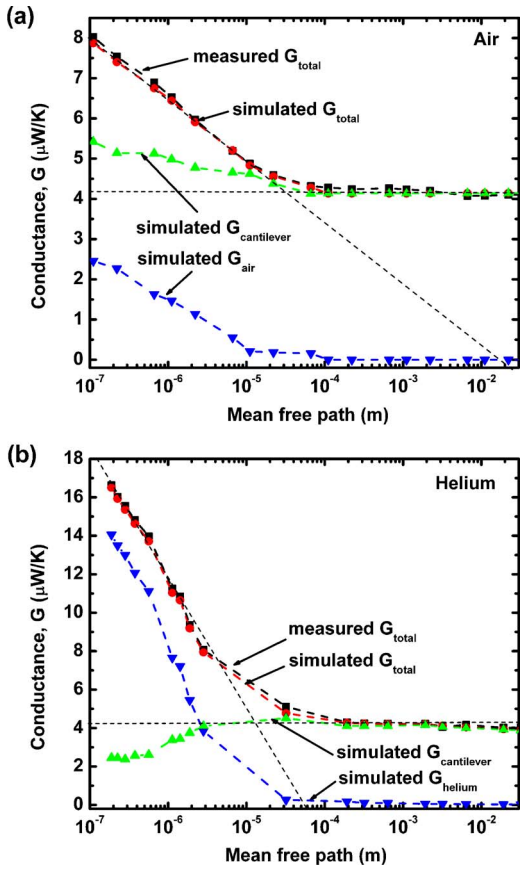

FIG. 7. (Color online) Simulated conductances show good agreement with measurements with a heated cantilever in (a) air and (b) helium. Finite difference heat transfer simulation fits the air conductance to cantilever power, electrical resistance, and temperature.

perimental values for conductance are simply the cantilever heating power divided by temperature difference between the heater and the UHV chamber. The simulated conductance was found as the best fit within the simulation to the experimentally measured temperature and power. Once the best fit was found, the total conductance from each node could be divided into both solid conductance along the cantilever and gas conductance. The plots of Fig. 7 show these values for both air and helium. Measured and simulated conductances are pressure dependent when $\mathrm{Kn}<1$ and become pressure independent when $\mathrm{Kn}>1$. Both air and helium show similar trend except for the solid conductance. While the solid conductance in air decreases, the solid conductance in helium increases with decreasing pressure.

When $\mathrm{Kn}<1$, simulated solid conductance is not constant since the temperature distribution along the cantilever depends on pressure. Simulation results using air as gas medium show that air conductance is 2.67 μW/K, corresponding to 1 mW power at atmospheric pressure. As pressure decreased, air conductance decreased to 0.155 μW/K or less at 1 mbar and below where it became negligible compared to solid conductance. For the helium, solid conductance also shows pressure dependence only when $\mathrm{Kn}<1$ and the simulated gas conductance varied between 13.76 μW/K at atmospheric pressure and 0.174 μW/K or less at 1 mbar and below.

To verify that thermal radiation was not significant, the simulations were performed with and without thermal radiation between the cantilever and the environment. The cantilever was assumed to be a blackbody and the radiative exchange between each node and the environment was evaluated using the Stefan-Boltzmann law.[16] From simulation, heat transfer due to thermal radiation was 20 μW and total power dissipation was 1.59 mW at high vacuum. Thermal radiation will not exceed 1.3% of the total power dissipation regardless of pressure when the cantilever heater temperature is held at 400 °C. At high vacuum, which is 10^{-5} mbar for air and 10^{-3} mbar for helium, thermal radiation will exceed 6.5% of the total power at 1000 °C. When operated in air at 1 atm, thermal radiation accounts for 0.5% of the total power when the cantilever heater region is 400 °C and thermal radiation will exceed 2% of the total power at 1000 °C. For operation in air at 1 atm, the cantilever temperature should exceed 1850 °C in order for thermal radiation to account for more than 10% of the dissipated power. This temperature would be well above the melting temperature of silicon.

For microfabricated Pirani gauges, the gap distance between heater and heat sink is typically considered as the characteristic length scale and the device size is overlooked since the gap distance is kept shorter than the heater size. In contrast, this study examines a device where the heater size has a dominant effect. While microfabricated Pirani sensors are designed to minimize solid conductance, the current microcantilevers have solid conductance comparable to or

higher than the gas conductance. The microcantilever exhibits its pressure-dependent power dissipation near atmospheric pressure, which is out of range for traditional Pirani gauges.

In this work, the heated microcantilever was configured in the UHV chamber with 500 μm separation so that the cantilever hardly feels the presence of the substrate. This heated cantilever needs to be located in proximity of the substrate and be engaged for application such as UHV-thermal dip-pen nanolithography. Since the presence of the substrate in proximity greatly affects heat transfer physics around the cantilever, more detailed experiments and simulations are required. The gap distance between the cantilever and the substrate will be much smaller than the heater size such that the gap distance will be the system characteristic length and used for the Kn number.

IV. CONCLUSION

This paper reports the thermal and electrical characteristics of a heated microcantilever in air and helium over a wide range of pressures. The cantilever heater size plays a key role in modulating thermal conduction between the cantilever and its gaseous surroundings. The change in the thermal conductance regime associated with a microcantilever heater can be universally described by the Knudsen number for different gas species. This measurement of thermal conductance around Kn=1 may aid the design of future micro-Pirani and other thermal MEMS sensors. Moreover, this work enables research into UHV applications of heated AFM cantilevers.

ACKNOWLEDGMENTS

The work was funded by NSF-NIRT, NSF-CAREER for WPK, and ONR.

[1] D. G. Cahill, W. K. Ford, K. E. Goodson, G. D. Mahan, A. Majumdar, H. J. Maris, R. Merlin, and S. R. Philpot, J. Appl. Phys. **93**, 793 (2003).
[2] R. Puers, S. Reyntjens, and D. De Bruyker, Sens. Actuators, A **97–98**, 208 (2002); M. Doms, A. Bekesch, and J. Mueller, J. Micromech. Microeng. **15**, 1504 (2005); J. Chae, B. H. Stark, and K. Najafi, IEEE Trans. Adv. Packag. **24**, 619 (2005).
[3] E. H. Kennard, *Kinetic Theory of Gases* (McGraw-Hill, New York, 1938).
[4] G. Binnig, M. Despont, U. Drechsler, W. Häberle, M. Lutwyche, P. Vettiger, H. J. Mamin, B. W. Chui, and T. W. Kenny, Appl. Phys. Lett. **76**, 1329 (1999).
[5] W. P. King, T. W. Kenny, K. E. Goodson, G. L. W. Cross, M. Despont, U. Dürig, H. Rothuizen, G. Binnig, and P. Vettiger, Appl. Phys. Lett. **78**, 1300 (2001); J. Microelectromech. Syst. **11**, 765 (2002).
[6] L. A. Pinnaduwage, A. Gehl, D. L. Hedden, G. Muralidharan, T. Thundat, R. T. Lareau, T. Sulchek, L. Manning, B. Rogers, M. Jones, and J. D. Adams, Nature (London) **425**, 474 (2003).
[7] W. P. King, T. W. Kenny, and K. E. Goodson, Appl. Phys. Lett. **85**, 2086 (2004).
[8] P. E. Sheehan, L. J. Whitman, W. P. King, and B. A. Nelson, Appl. Phys. Lett. **85**, 1589 (2004); B. A. Nelson, W. P. King, A. R. Laracuente, P. E. Sheehan, and L. J. Whitman, Appl. Phys. Lett. **88**, 033104 (2006).
[9] A. Passian, A. Wig, F. Meriaudeau, T. L. Ferrell, and T. Thundat, J. Appl. Phys. **92**, 6326 (2002); A. Passian, R. J. Warmack, T. L. Ferrell, and T. Thundat, Phys. Rev. Lett. **90**, 124503 (2003); B. Gotsmann and U. Dürig, Appl. Phys. Lett. **87**, 194102 (2005); N. Masters, W. Ye, and W. P. King, Phys. Fluids **17**, 100615 (2005).
[10] B. W. Chui, T. D. Stowe, Y. S. Ju, K. E. Goodson, T. W. Kenny, H. J. Mamin, B. D. Terris, and R. P. Ried, J. Microelectromech. Syst. **7**, 69 (1998).
[11] J. Lee, T. Beechem, T. L. Wright, B. A. Nelson, S. Graham, and W. P. King, J. Microelectromech. Syst. (in press).
[12] B. W. Chui, M. Asheghi, Y. S. Ju, K. E. Goodson, T. W. Kenny, and H. J. Mamin, Microscale Thermophys. Eng. **3**, 217 (1999).
[13] M. R. Abel, T. L. Wright, W. P. King, and S. Graham, IEEE Trans. Compon. Packag. Technol. (in press).
[14] E. O. Sunden, T. L. Wright, J. Lee, W. P. King, and S. Graham, Appl. Phys. Lett. **88**, 033107 (2006).
[15] W. P. King, J. Micromech. Microeng. **15**, 2441 (2005).
[16] F. P. Incropera and D. P. DeWitt, *Fundamentals of Heat and Mass Transfer*, 4th ed. (Wiley, New York, 2002).
[17] W. J. Liu, K. Etessam-Yazdani, R. Hussin, and M. Asheghi, IEEE Trans. Electron Devices **53**, 1868 (2006).